Updated High-Temperature Opacities for The Dartmouth Stellar Evolution Program and their Effect on the Jao Gap Location

Thomas M. Boudreaux[1] and Brian C. Chaboyer[1]

[1]*Department of Physics and Astronomy, Dartmouth College, Hanover, NH 03755, USA*

ABSTRACT

The Jao Gap, a 17 percent decrease in stellar density at $M_G \sim 10$ identified in both Gaia DR2 and EDR3 data, presents a new method to probe the interior structure of stars near the fully convective transition mass. The Gap is believed to originate from convective kissing instability wherein asymmetric production of He^3 causes the core convective zone of a star to periodically expand and contract and consequently the stars' luminosity to vary. Modeling of the Gap has revealed a sensitivity in its magnitude to a population's metallicity primarily through opacity. Thus far, models of the Jao Gap have relied on OPAL high-temperature radiative opacities. Here we present updated synthetic population models tracing the Gap location modeled with the Dartmouth stellar evolution code using the OPLIB high-temperature radiative opacities. Use of these updated opacities changes the predicted location of the Jao Gap by ~ 0.05 mag as compared to models which use the OPAL opacities.

Keywords: Stellar Evolution (1599) — Stellar Evolutionary Models (2046)

1. INTRODUCTION

Jao et al. (2018) discovered a novel feature in the Gaia $G_{BP} - G_{RP}$ color-magnitude-diagram. Around $M_G = 10$ there is an approximately 17% decrease in stellar density of the sample of stars Jao et al. considered. Subsequently, this has become known as either the Jao Gap, or Gaia M dwarf Gap. Section ?? will go into more detail regarding the physics underpinning this feature; however, in brief convective instabilities in the core are believed to form for stars straddling the fully convective transition mass (0.3 - 0.35 $M_\odot$) (Baraffe & Chabrier 2018). These instabilities interupt the normal, slow, main sequence luminosity evolution of a star and resulting in lower than expected luminosities [WORD-ING] (Jao & Feiden 2020).

The Jao Gap, inherently a feature of M dwarf populations, provides an enticing and unique view into the interior physics of these stars (Feiden et al. 2021). This is especially important as, unlike more massive stars, M dwarf seismology is currently infeasible due to the short periods and extremely small magnitude's which both ra-

Corresponding author: Thomas M. Boudreaux

thomas.m.boudreaux.gr@dartmouth.edu,
thomas@boudreauxmail.com

dial and low-order low-degree non-radial seismic waves are predicted to have in such low mass stars (Rodríguez-López 2019). The Jao Gap therefore provides one of the only current methods to probe the interior physics of M dwarfs.

Stellar modeling has been successful in reproducing the Jao Gap (e.g. Feiden et al. 2021; Mansfield & Kroupa 2021) and, with these models, we have begun to understand which parameters constrain the Jao Gap's location. For example, it is now well documented that metallicity affects the Jao Gap's color, with higher metallicity stellar populations showing the Jao Gap at consistently higher masses / bluer colors (Mansfield & Kroupa 2021).

2. JAO GAP

A theoretical explanation for the Jao Gap (Figure 1) comes from van Saders & Pinsonneault (2012), who propose that in a star directly above the transition mass, due to asymmetric production and destruction of He^3 during the proton-proton I chain (ppI), periodic luminosity variations can be induced. This process is known as convective-kissing instability. Such a star will descend the pre-main sequence with a radiative core; however, as the star reaches the zero age main sequence (ZAMS) and as the core temperature exceeds 7×10^6 K, enough energy will be produced by the ppI chain that the core becomes convective. At this point the star exists with
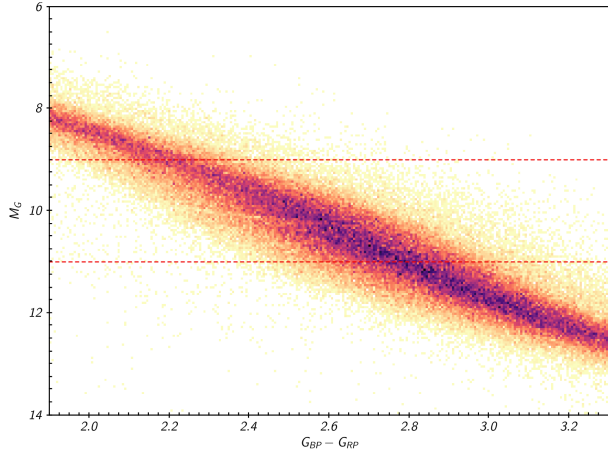
Figure 1. Figure 1 from Jao et al. (2018) showing the so called "Jao Gap" at $M_G \approx 10$ [SHOULD I REMAKE THIS USING DR3 DATA?]

both a convective core and envelope, in addition to a thin, radiative, layer separating the two. Subsequently, asymmetries in ppI affect the evolution of the star's convective core.

The proton-proton I chain constitutes three reactions

1. $p + p \longrightarrow d + e^+ + \nu_e$

2. $p + d \longrightarrow {}^3\text{He} + \gamma$

3. ${}^3\text{He} + {}^3\text{He} \longrightarrow {}^3\text{He} + 2p$

Because reaction 3 of ppI consumes ^{3}He at a slower rate than it is produced by reaction 2, ^{3}He abundance increases in the core increasing energy generation. The core convective zone will therefore expand as more of the star becomes unstable to convection. This expansion will continue until the core connects with the convective envelope. At this point convective mixing can transport material throughout the entire radius of the star and the high concentration of ^{3}He will rapidly diffuse outward, away from the core, again decreasing energy generation as reaction 3 slows down. Ultimately, this leads to the convective region around the core pulling back away from the convective envelope, leaving in place the radiative transition zone, at which point ^{3}He concentrations build up in the core until it once again expands to meet the envelope. This process repeats until the He^3 concentration throughout the star is enough such that the core can sustain nuclear reaction rates which keep it in with the envelope, resulting in a fully convective star.

2.1. *Modeling the Gap*

Since the identification of the Gaia M-dwarf gap, stellar modeling has been conducted to better constrain its location, effects, and exact cause. Both Mansfield &

Kroupa (2021) and Feiden et al. (2021) identify that the gap's mass location is correlated with model metallicity — the mass-luminosity discontinuity in lower metallicity models being at a commensurately lower mass. Feiden et al. (2021) suggests this dependence is due to the steep relation of the radiative temperature gradient, ∇_{rad}, on temperature and in turn, on stellar mass.

$$\nabla_{rad} \propto \frac{L\kappa}{T^4} \qquad (1)$$

As metallicity decreases so does opacity, which, by Equation 1, dramatically lowers the temperature where radiation will dominate energy transport (Chabrier & Baraffe 1997). Since main sequence stars are virialized the core temperature is proportional to the core density and total mass (Equation 2). Therefore, if the core temperature where convective-kissing instability is expected decreases with metallicity, so too will the mass of stars which experience such instabilities.

$$T_c \propto \rho_c M^2 \qquad (2)$$

This strong opacity dependence presents a slight problem where modeling is concerned. With current computational tools it is infeasible to compute opacities on the fly; rather, Rossland Mean opacity (κ_R) for individual elements must be pre-tabulated over a wide range of temperatures and densities. These opacities can then be somewhat arbitrarily mixed together and interpolated to form opacity lookup-tables. Multiple groups have performed these calculations and subsequently made tables available to the wider community, these include the Opacity Project (OP Seaton et al. 1994), Laurence Livermore National Labs OPAL opacity tables (Iglesias & Rogers 1996), and Los Alamos National Labs OPLIB opacity tables (Colgan et al. 2016).

3. UPDATED OPACITIES

OPAL high-temperature radiative opacity tables in particular are very widely used by current generation isochrone grids (e.g. Dartmouth, MIST, & StarEvol, Dotter et al. 2008; Choi et al. 2016; Amard et al. 2019). However, there are two primary issues with these tables, one, they are relativly old and therefore do not incorperate the most up to date understanding of plasma modeling in their code [CITATION], and two, they report rossland mean opacitieis to only N digits [WHICH IS AN ISSUE WHY?].

While the two issues given above should have relativly small affects, the strong theoretical opacity dependence of the Jao Gap raises the potential for these small effects

to measurably shift the gap's location. In order to address both the out of date plasma modeling and the low numeric presicion we update DSEP to use high temperature opacity tables based on measurements from Los Alamos national Labs T-1 group (OPLIB, Colgan et al. 2016). The OPLIB tables use the much more up-to-date ATOMIC plasma modeling code [CITATION] in addition to reporting rossland mean opacities to N digits of numeric presicion.

ATOMIC (Magee et al. 2004) is a LTE and non-LTE opacity and plasma modeling code. A major strength of ATOMIC when compared to the older plasma modeling programs is its ability to vary its refinement level (Fontes et al. 2015). [OTHER DIFFERENCES] For a more detailed breakdown of how the most up-to-date set of OPLIB tables are generated see (Colgan et al. 2016).

The most up to date OPLIB tables include monochromatic Rosseland mean opacities — composed from bound-bound, bound-free, free-free, and scattering opacities — for elements hydrogen through zinc over temperatures 0.5eV to 100 keV and for mass densities from approximately 10^{-8} g cm^{-3} up to approximately 10^4 g cm^{-3} (though the exact mass density range varies as a function of temperature).

When comparing OPAL and OPLIB opacity tables (Figure 2) we find OPLIB opacities are systematically lower than OPAL opacities for temperature above 10^6 K (Figure 2). These lower opacities will result the temperature where radiation dominates energy transport lowering [CITATION?]. Consequently, the radiative layer in stellar models evolved using OPLIB opacity tables will be [further?] out from the models center than it would be in models making use of OPAL tables.

3.1. *Table Querying and Conversion*

DSEP, along with most other stellar evolution programs, uses pre-computed high-temperature opacity tables. Specifically, these tables list the Rosseland-mean opacity, κ_R, along three dimensions: temperature, a density proxy R, and composition. R is defined as

$$R = \frac{\rho}{T_6^3} \qquad (3)$$

Where $T_6 = T \times 10^{-6}$ and ρ is the mass density. If T and ρ are given in cgs then for much of the radius of a star $\log(R) \sim -1.5$ [CITATION]. R is used, as opposed to simply tracking opacity over mass density, because of its small dynamic range when compared to ρ ($\rho \sim 10^5$ [g cm^{-3}] at the core of an RGB star all the way down to $\sim 10^{-8}$ [g cm^{-3}] within the envelope).
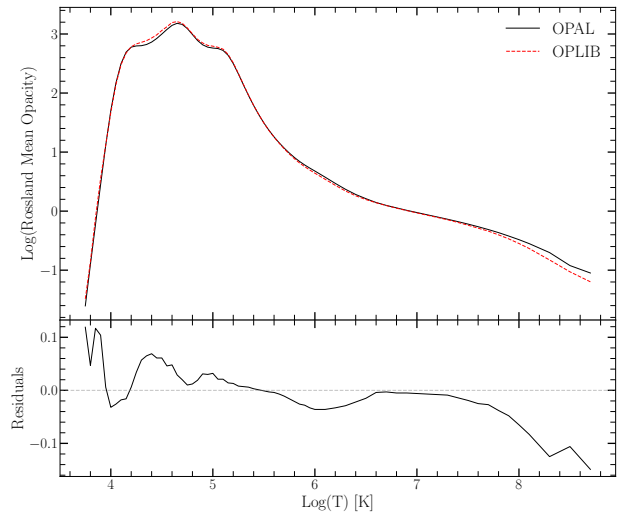
Figure 2. Rosseland mean opacity with the GS98 solar composition for both OPAL opacities and OPLIB opacities (top). Residuals between OPLIB opacities and OPAL opacities (bottom). These opacities are plotted at $\log_{10}(R) = -1.5$, $X = 0.7$, and $Z = 0.02$. Note how the OPLIB opacities are systematically lower than the OPAL opacities for temperatures above 10^6 K.

OPLIB tables are queried from a web interface[1]. In order to generate many tables easily and quickly we develop a web scraper built with Python's `requests` module in addition to the 3rd party `mechanize` and `BeautifulSoup` modules (Chandra & Varanasi 2015; Richardson 2007) which can get tables with minimal intervention. This web scraper submits a user requested chemical composition (composed of mass fractions for elements from Hydrogen to Zinc) to the Los Alamos web form, selects 0.0005 keV as the lower temperature bound and 60 keV as the upper temperature bound, and finally requests opacity measurements for 100 densities, ranging from $1.77827941 \times 10^{-15}$ [g cm^{-3}] up to 1×10^7 [g cm^{-3}], at each temperature interval. These correspond to approximately the same temperature and density range of opacities present in the OPAL opacity tables.

OPLIB reports κ_R as a function of mass density, temperature in keV, and composition. Recall that DSEP accepts tables where opacity is given as a function of temperature in Kelvin, R, and composition. The conversion from temperature in keV to Kelvin is trivial

$$T_K = T_{keV} * 11604525.0061657 \qquad (4)$$

However, the conversion from mass density to R is more involved. Because R is coupled with both mass

---

[1] https://aphysics2.lanl.gov/apps/

density and temperature there there is no way to directly convert tabulated values of opacity reported in the OPLIB tables to their equivalents in R space. Instead we must rotate the tables, interpolating $\kappa_R(\rho, T_{eff}) \rightarrow \kappa_R(R, T_{eff})$.

To preform this rotation we use the `interp2d` function within `scipy`'s `interpolate` (Virtanen et al. 2020) module to construct a cubic bivariate B-spline (DIERCKX 1981) interpolating function s, with a smoothing factor of 0, representing the surface $\kappa_R(\rho, T_{eff})$. For each R^i and T_{eff}^j which DSEP expects high-temperature opacities to be reported for, we evaluate Equation 3 to find $\rho^{ij} = \rho(T_{eff}^j, R^i)$. Opacities in T_{eff}, R space are then inferred as $\kappa_R^{ij}(R^i, T_{eff}^j) = s(\rho^{ij}, T_{eff}^j)$.

As first-order validation of this interpolation scheme we can preform a similar interpolation in the opposite direction, rotating the tables back to $\kappa_R(\rho, T_{eff})$ and then comparing the initial, "raw", opacities to those which have gone through the interpolations process. Figure 3 shows the fractional difference between the raw opacities and a set which have gone through this double interpolation. The red line denotes $Log(R) = -1.5$ where models will tend to sit for much of their radius. Along the $Log(R) = -1.5$ line the mean fractional difference is $\langle \delta \rangle = 0.006$ with an uncertainty of $\sigma_{\langle \delta \rangle} = 0.009$. One point of note is that, because the initial rotation into $Log(R)$ space also reduces the domain of the opacity function interpolation-edge effects which we avoid initially by extending the domain past what DSEP needs cannot be avoided when interpolating back into ρ space. [IS THERE SOME MORE CLEAR VALIDATION WHICH I SHOULD PREFORM?]

4. SOLAR CALIBRATED STELLAR MODELS

In order to validate the OPLIB opacities, we generate a solar calibrated stellar model (SCSM) using these new tables. We allow both the convective mixing length parameter, α_{ML}, and the initial Hydrogen mass fraction, X, to vary simultaniously, minimizeing the difference between resultant models' final radius and luminosity to those of the sun.

Optimization of α_{ML} and X is conducted using gradient descent. For each optimization step three models are evolved: a reference model, a model with a small perturbation to the hydrogen mass fraction but the same mixing length as the reference model, and a model with a small perturbation to the mixing length but the same hydrogen mass fraction as the reference. Perturbations are sampled from a normal distribution (implemented though `numpy.random`). This distribution is sampled and that sample is then added to the reference value for either X or α_{ML}. The luminosity and radius of the
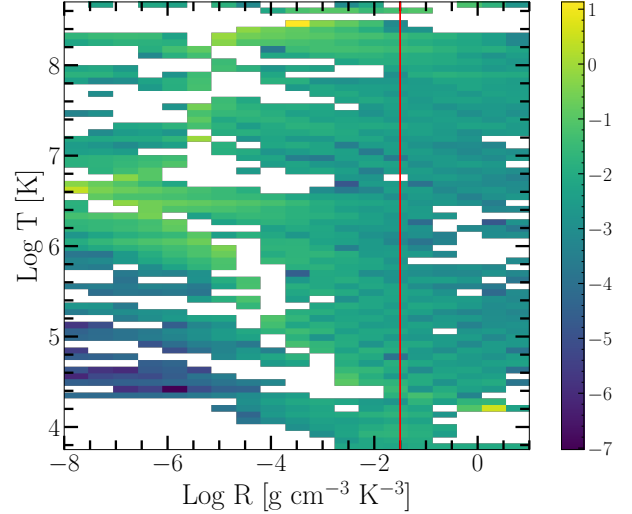
Figure 3. Log Fractional Difference between opacities in $\kappa_R(\rho, T_{eff})$ space directly queried from the OPLIB webform and those which have been interpolated into $Log(R)$ space and back. Note that, due to the temperature grid DSEP uses not aligning perfectly which the temperature grid OPLIB uses there may be edge effects where the interpolation is poorly constrained. The red line corresponds to $Log(R) = -1.5$ where much of a stellar model's radius exists.
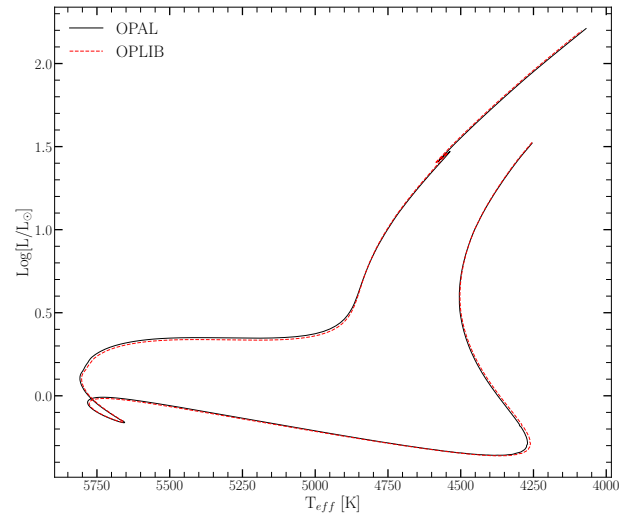
Figure 4. HR Diagram for the two SCSMs, OPAL and OPLIB. OPLIB is show as a grey dashed line.

three evolved models are compared to solar values and the gradient of the resultant $L - L_\odot$, $R - R_\odot$ surface is followed down to new estimates for the reference values of X and α_{ML}. This process is is repeated until the difference between successive X and α_{ML} drops below one part in 10^5.

Solar calibrated stellar models evolved using GS98 OPAL and OPLIB opacity tables (Figure 4) differ $\sim$ 0.5% in the SCSM hydrogen mass fractions and $\sim 1.5\%$

Model	X	α_{ML}
OPAL	0.7066	1.9333
OPLIB	0.7107	1.9629

Table 1. Optimized parameters for SCSMs evolved using OPAL and OPLIB high temperature opacity tables.

in the SCSM convective mixing length parameters (Table 1). While the two evolutionary tracks are very similar, note that the OPLIB SCSM's luminosity is systematically lower at the same effective temperature all the way from the premain sequence up and until the star leaves the main sequence, at which point it is effectively the same as the OPAL SCSM. This luminosity difference between OPAL and OPLIB based models is consistent with expectations given the steeper temperature gradient the lower OPLIB opacities will result in.

5. MODELING

In order to model the Jao Gap we evolve two extremly finely sampled mass grid of models. One of these grids uses the OPAL high-temperature opacity tables while the other uses the OPLIB tables. Each grid evolves a model every 0.00025 $M_\odot$ from 0.2 to 0.4 $M_\odot$ and every 0.005 $M_\odot$ from 0.4 to 0.8 $M_\odot$. All models in both grids use a GS98 solar composition, the (1, 101, 0) `Free_EOS` (version 2.7) configuration, and 1000 year old pre-main sequence polytropic models as their initial conditions.

Because in this work we are just interested in the location shift of the gap as the opacity source varies, we do not model variations in composition. Others have done this and they have found blah....

The variability leading to the gap is quite clear in the mass luminosity relation (Figures 5 & 6 Make this figure for the two large runs)

5.1. *Population Synthethis*

In order to compare the gap to observations we use in house population synthetis code. Our population synthetis code first uses inverse CDF sampling to build a distribution of target masses from some initial mass function (IMF). Specifically we use the Sollima IMF where, for masses 0.25 $M_\odot$ ¡ M ¡ 1 $M_\odot$, $\alpha = -1.34 \pm 0.07$. The model nearest in mass to the samples mass above and the nearest model below are then selected from the evolved database. The surface gravity, luminosity, and effective temperature of the sample are then estimated through computing a linear interpolation between the bounding models and evaluating that interpolation at the sample mass. T_{eff}, g, and $log(L)$ are transformed into Gaia G, BP, and RP magnitudes using the bolometric corrections provided by the Gaia Colaboration, specifically `fehp000.UBVRIplus` [CITATION] [How to
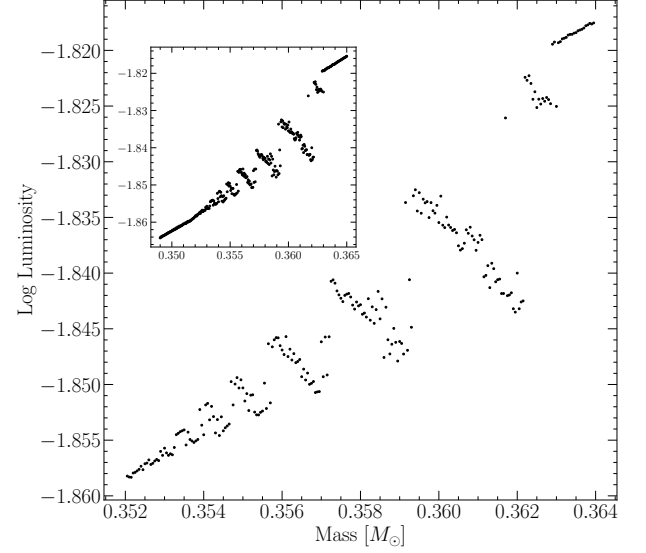
Figure 5. THIS IS A TEST FIGURE, REPLACE WHEN LARGE RUN IS DONE
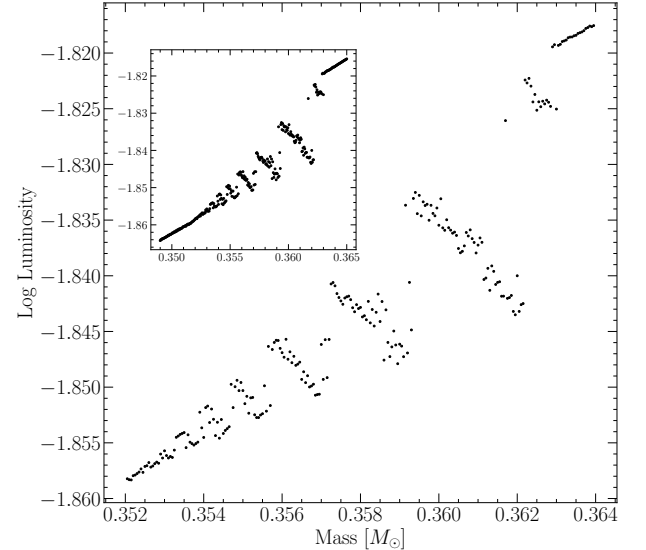
Figure 6. THIS IS A TEST FIGURE, REPLACE WHEN LARGE RUN IS DONE

cite Aarons code]. Next, we introduce observationally informed photometric and astrometric Uncertainties into our population.

We select the Gaia Catalogue of Nearby Stars (GCNS) [CITATION] to empirically calibrate uncertainty relations. A function with the form of Equation 5 is fit to parallax uncertainty vs. G magnitude. Additionally, a function of the form of Equation 6 is fit to to ith (G, BP, RP) magnitude uncertainty vs. ith magnitude.

$$\sigma_{plx}(M_g) = ae^{bM_g} + c \qquad (5)$$

$$\sigma_i(M_i) = ae^{M_i - b} + c \qquad (6)$$

Each of these functions then gives the an estimated uncertainty of some quantity at a given magnitude. For each sampled star in the synthetic population we select a parallax from the GCNS, refered to as the "true parallax". This selection follows the distribution given in Figure MAKE A FIGURE PLOTTING p from from-Tagger.py in ThomasAstro on line 39 in that file. A parallax uncertainty is calculated based on the G magnitude magnitude of the synthetic star (hereafter the "true G magnitude) and the results of the fitting described in the previous paragraph. This uncertainty then will, with equal weighting, either be added or subtracted from the true parallax, yeilding an "observed parallax". The true parallax will be used to convert the true i$^{\text{th}}$ magnitude to an apparent i$^{\text{th}}$ magnitude and the observed parallax will be used to convert the apparent i$^{\text{th}}$ magnitude into an observed i$^{\text{th}}$ magnitude. Finally, each observed magnitude is summed with an estimated uncertainty for that magnitude based on the fit of the i$^{\text{th}}$ magnitude to the uncertainty in the i$^{\text{th}}$ magnitude.

To summarize the process that each synthetic star will go through

1. Sample from a Sollima (2019) IMF to determine synthetic star mass

2. Find the closest model above and below the synthetic star, linerally interpolate model parameters to the synthetic star mass.

3. Convert synthetic star g, T_{eff}, and $Log(L)$ to Gaia G, BP, and RP colors.

4. Sample from the GCNS to assign synthetic star a "true" parallax.

5. Evaluate the empirical calibration given in Equation 5 to find an associated parallax uncertainty and adjust the true parallax by this value resulting in an observed parallax.

6. Use the true parallax to find an apparent magnitude for each filter.

7. Use the observed parallax and the apparent magnitude to find an observed magnitude

8. Evaluate the empirical calibration given in Equation 6 to give a magnitude uncertainty scale in each band.

9. Adjust each magnitude by some amount sampled from a normal distribution with a standard deviation of the magnitude uncertainty scale.

This method then incorperats both photometric and astrometric Uncertainties into our population synthetis.

Talk about how you locate the gap formally, there should be a figure for this as well.

6. RESULTS

Talk About results of population synthetis, i.e. where the gap is in OPAL vs OPLIB, show the CMD

Then compare the results to observations, comment on which one matches observations better and also how confident we can be about that

Comment on if the shift in the gap location is larger or smaller than the size o fthe gap or the shift due to other effects such as variations in age or composition, i.e is it Significant enough to matter

comment on why the gap shifts in the manner which it does, i.e the opacities are lower. Show how for a constant opacity table increasing the metallicity (which will also change the opacity) affetcs the gap location)

7. CONCLUSION

REFERENCES

Amard, L., Palacios, A., Charbonnel, C., et al. 2019, A&A, 631, A77, doi: 10.1051/0004-6361/201935160

Baraffe, I., & Chabrier, G. 2018, A&A, 619, A177, doi: 10.1051/0004-6361/201834062

Chabrier, G., & Baraffe, I. 1997, A&A, 327, 1039. https://arxiv.org/abs/astro-ph/9704118

Chandra, R. V., & Varanasi, B. S. 2015, Python requests essentials (Packt Publishing Ltd)

Choi, J., Dotter, A., Conroy, C., et al. 2016, ApJ, 823, 102, doi: 10.3847/0004-637X/823/2/102

Colgan, J., Kilcrease, D. P., Magee, N. H., et al. 2016, in APS Meeting Abstracts, Vol. 2016, APS Division of Atomic, Molecular and Optical Physics Meeting Abstracts, D1.008

DIERCKX, P. 1981, IMA Journal of Numerical Analysis, 1, 267, doi: 10.1093/imanum/1.3.267

Dotter, A., Chaboyer, B., Jevremović, D., et al. 2008, The Astrophysical Journal Supplement Series, 178, 89

Feiden, G. A., Skidmore, K., & Jao, W.-C. 2021, ApJ, 907, 53, doi: 10.3847/1538-4357/abcc03

Fontes, C. J., Zhang, H. L., Abdallah, J., J., et al. 2015, Journal of Physics B Atomic Molecular Physics, 48, 144014, doi: 10.1088/0953-4075/48/14/144014

Iglesias, C. A., & Rogers, F. J. 1996, ApJ, 464, 943, doi: 10.1086/177381

Jao, W.-C., & Feiden, G. A. 2020, AJ, 160, 102, doi: 10.3847/1538-3881/aba192

Jao, W.-C., Henry, T. J., Gies, D. R., & Hambly, N. C. 2018, ApJL, 861, L11, doi: 10.3847/2041-8213/aacdf6

Magee, N. H., Abdallah, J., Colgan, J., et al. 2004, in American Institute of Physics Conference Series, Vol. 730, Atomic Processes in Plasmas: 14th APS Topical Conference on Atomic Processes in Plasmas, ed. J. S. Cohen, D. P. Kilcrease, & S. Mazavet, 168–179

Mansfield, S., & Kroupa, P. 2021, A&A, 650, A184, doi: 10.1051/0004-6361/202140536

Richardson, L. 2007, April

Rodríguez-López, C. 2019, Frontiers in Astronomy and Space Sciences, 6, 76, doi: 10.3389/fspas.2019.00076

Seaton, M. J., Yan, Y., Mihalas, D., & Pradhan, A. K. 1994, MNRAS, 266, 805, doi: 10.1093/mnras/266.4.805

Sollima, A. 2019, Monthly Notices of the Royal Astronomical Society, 489, 2377, doi: 10.1093/mnras/stz2093

van Saders, J. L., & Pinsonneault, M. H. 2012, ApJ, 751, 98, doi: 10.1088/0004-637X/751/2/98

Virtanen, P., Gommers, R., Oliphant, T. E., et al. 2020, Nature Methods, 17, 261, doi: 10.1038/s41592-019-0686-2